Cell

Specificity of ARGONAUTE7-miR390 Interaction and Dual Functionality in *TAS3 Trans*-Acting siRNA Formation

Taiowa A. Montgomery,[1,2] Miya D. Howell,[2,3] Josh T. Cuperus,[1,2] Dawei Li,[4] Jesse E. Hansen,[2] Amanda L. Alexander,[2] Elisabeth J. Chapman,[1,2,5] Noah Fahlgren,[1,2] Edwards Allen,[2,3,6] and James C. Carrington[2,3,*]
[1]Molecular and Cellular Biology Program
[2]Department of Botany and Plant Pathology
[3]Center for Genome Research and Biocomputing
Oregon State University, Corvallis, OR 97331, USA
[4]State Key Laboratory for Agro-Biotechnology, China Agricultural University, Beijing 100094, China
[5]Present address: Department of Biology, Indiana University, Bloomington, IN 47405, USA.
[6]Present address: Monsanto Company, Chesterfield, MO 63017, USA.
*Correspondence: carrington@cgrb.oregonstate.edu
DOI 10.1016/j.cell.2008.02.033

SUMMARY

Trans-acting siRNA form through a refined RNAi mechanism in plants. miRNA-guided cleavage triggers entry of precursor transcripts into an RNA-DEPENDENT RNA POLYMERASE6 pathway, and sets the register for phased tasiRNA formation by DICER-LIKE4. Here, we show that miR390-ARGONAUTE7 complexes function in distinct cleavage or noncleavage modes at two target sites in *TAS3a* transcripts. The AGO7 cleavage, but not the noncleavage, function could be provided by AGO1, the dominant miRNA-associated AGO, but only when AGO1 was guided to a modified target site through an alternate miRNA. AGO7 was highly selective for interaction with miR390, and miR390 in turn was excluded from association with AGO1 due entirely to an incompatible 5′ adenosine. Analysis of AGO1, AGO2, and AGO7 revealed a potent 5′ nucleotide discrimination function for some, although not all, ARGONAUTEs. miR390 and AGO7, therefore, evolved as a highly specific miRNA guide/effector protein pair to function at two distinct tasiRNA biogenesis steps.

INTRODUCTION

miRNA and tasiRNA are distinct classes of small RNAs that guide silencing of target RNAs through cleavage or nondegradative repression mechanisms (Chapman and Carrington, 2007). miRNAs arise from transcripts that adopt imperfect, self-complementary foldback structures, whereas tasiRNAs arise from a refined adaptation of the RNAi pathway. *TAS* transcripts are first processed by miRNA-guided cleavage, which forms a discrete 5′ or 3′ end, and then transcribed by RNA-DEPENDENT RNA POLYMERASE6 (RDR6). The resulting dsRNA is processed into siRNA duplexes in end-dependent, 21 nucleotide steps by DICER-LIKE4 (DCL4) (Allen et al., 2005; Gasciolli et al., 2005; Peragine et al., 2004; Vazquez et al., 2004; Xie et al., 2005; Yoshikawa et al., 2005). Effector complex formation involves strand separation and selective association with an ARGONAUTE (AGO) protein.

Arabidopsis contains four characterized *TAS* gene families. *TAS1*, *TAS2,* and *TAS4* tasiRNA biogenesis initiates with miR173- (*TAS1* and *TAS2*) or miR828-guided (*TAS4*) cleavage on the 5′ side of the tasiRNA-generating region, while *TAS3* tasiRNAs form by miR390-guided cleavage on the 3′ side. miR390 also interacts in a noncleavage mode with a second site near the 5′ end (Axtell et al., 2006; Howell et al., 2007). Features of the *TAS3* family, including targeting by miR390, are highly conserved in land plants (Allen et al., 2005; Axtell et al., 2006, 2007; Talmor-Neiman et al., 2006). *TAS3* tasiRNAs, but not those from *TAS1* or *TAS2*, are dependent on a specialized ARGONAUTE, AGO7 (also called ZIP) (Adenot et al., 2006; Fahlgren et al., 2006; Hunter et al., 2006). *TAS3* tasiRNAs target mRNAs encoding several AUXIN RESPONSE FACTORs (ARF3 and ARF4), negative regulation of which is necessary for proper developmental timing and lateral organ development along the adaxial-abaxial axis (Adenot et al., 2006; Fahlgren et al., 2006; Garcia et al., 2006; Hunter et al., 2006).

The mechanisms for recognition and routing of transcripts through the tasiRNA or RDR6/DCL4-dependent pathway are not well understood. Axtell et al. (2006) proposed a two-hit trigger mechanism, in which transcripts with two or more small RNA target sites are preferentially routed into the RDR6/DCL4 pathway. This explains some aspects of *TAS3* tasiRNA formation and the routing of several known, multiply targeted transcripts (Axtell et al., 2006; Chen et al., 2007; Howell et al., 2007), although not necessarily *TAS1*, *TAS2*, and *TAS4* tasiRNA biogenesis. How the factors associated with miR828, miR173, and miR390 function to provide routing information remains an unresolved problem. In this paper, we show that miR390 is uniquely adapted to initiate *TAS3* tasiRNA biogenesis due to

its specific association with AGO7, and that AGO7-miR390 complexes function in two distinct modes to process and route transcripts through the RDR6/DCL4 pathway. We also found an AGO function that discriminates among small RNAs on the basis of 5′ nucleotide identity.

RESULTS

Design and Validation of Syn-tasiRNAs

Based on the predictable phased pattern of tasiRNA formation from the miR390-guided cleavage site, we generated *TAS3a*-based synthetic (syn)-tasiRNAs to silence the *Arabidopsis PHYTOENE DESATURASE* (*PDS*) transcript. Silencing of *PDS* mRNA results in photobleaching of green tissues (Kumagai et al., 1995). Canonical targeting rules were followed for syn-tasiRNA development, including incorporation of a 5′U and perfect complementarity between syn-tasiRNA nucleotides 2–13 (from the 5′ end) and the mRNA target (Allen et al., 2005; Jones-Rhoades and Bartel, 2004; Schwab et al., 2005). Two 35S promoter-driven *TAS3a*-based constructs (*35S:TAS3aPDS-1* and *35S:TAS3aPDS-2*) with tandem syn-tasiRNAs in the 5′ D7[+] and 5′ D8[+] positions (Allen et al., 2005) were developed (Figure 1A). These positions normally yield tasiR2141 and tasiR2142, which target *ARF* transcripts.

In Col-0 (wild-type, wt) plants expressing *35S:TAS3aPDS-1* and *35S:TAS3aPDS-2*, photobleaching emanated from the midrib and major veins and was more apparent from the adaxial side (Figure 1B). *PDS* mRNA accumulation was suppressed by 33% in *35S:TAS3aPDS-1*-transformed plants and 50% in *35S:TAS3aPDS-2*-transformed plants, but was suppressed to a slightly greater extent in midrib tissue compared to nonmidrib leaf tissue ($p < 0.05$; Figures 1C and 1D). Cotyledons displayed photobleaching that emanated from the apex along the petiole (Figure 1B). Mild photobleaching was also detected in flowers and siliques of *35S:TAS3aPDS-2*-transformed plants. Syn-tasiRNAs and the photobleaching phenotype were RDR6-, DCL4-, and AGO7 (ZIP)-dependent (Figures 1B and 1E; Table 1). *PDS* mRNA levels were not significantly different between Col-0 vector-transformed plants and *rdr6-15*, *dcl4-2*, and *zip-1 35S:TAS3aPDS-2*-transformed plants (p values between 0.26–0.86, two-sample t tests; Figure 1C). These results are consistent with the genetic requirements of *TAS3* tasiRNA, indicating that the syn-tasiRNA system faithfully reflects the endogenous pathway.

Limited Activity and Expression of AGO7

Plants expressing *35S:TAS3aPDS-1* and *35S:TAS3aPDS-2* displayed strongest photobleaching in vasculature-proximal tissue. To determine if expression patterns of known *TAS3*-specific factors explain this pattern, promoter-*GUS* fusion constructs were developed with *TAS3a*, *MIR390a*, *MIR390b*, and *AGO7* promoters. The GUS activity patterns in seedlings expressing *TAS3a:GUS*, *MIR390a:GUS*, and *MIR390b:GUS* were similar to the patterns of activity driven by the 35S promoter (*35S:GUS*). In contrast, seedlings expressing *AGO7:GUS* had activity that was detected primarily in the vasculature (Figure 1F). Syn-tasiRNA formation was tested in the presence or absence of ectopic AGO7 in *N. benthamiana* leaves. When transiently coexpressed with *35S:MIR390a* or *35S:MIR390b*, the *35S:TAS3aPDS-2* construct failed to yield syn-tasiRNA (Figure 1H; lanes 7 and 8). But when coexpressed with *35S:MIR390a* or *35S:MIR390b* and a 35S-promoter driven *AGO7* construct (*35S:HA-AGO7*; Figure 1G), *35S:TAS3aPDS-2* yielded relatively high levels of syn-tasiRNA (Figure 1H; lanes 9 and 10). The partial overlap between *AGO7* promoter activity and *TAS3a*-based syn-tasiRNA activity and the ability of constitutively active AGO7 to overcome limitations to syn-tasiRNA formation in *N. benthamiana* leaves suggest that AGO7 is limiting in leaves.

Distinct Roles for miR390 at the *TAS3a* 5′ and 3′ Target Sites

TAS3 tasiRNAs originate from sequences between two miR390 target sites. In flowering plants, but not in moss or pine, the miR390-target interaction at the 5′ proximal site contains key mispairs that prevent cleavage, and conversion to a cleavable miR390 target site inactivates the *TAS3a* locus (Axtell et al., 2006). In contrast, the 3′ proximal site is cleaved across plant species (Axtell et al., 2006). The unique roles of miR390 at the two target sites were analyzed with single and combination target site substitutions using *35S:TAS3aPDS-1* and *35S:TAS3aPDS-2* in Col-0 and *zip-1* plants. The 3′ site substitutions generated miR171 or miR159 sites, or a nonrecognized site (Figures 2A and S1A). The 5′ substitutions yielded an authentic, cleavable miR171 site, or target sites for five miRNAs that approximated the characteristics of the noncleavable miR390/*TAS3a* 5′ target interaction, including mispairs or G:U pairs at positions 9, 10, and 11 of the miRNA (Figures 2A and S2A; Table S1). A construct with 5′ site substitutions that destroyed targeting was also generated (Figure S2A). A dual target site substitution construct contained cleavable versions of miR171 target sites (Figure 2A).

The 3′ and 5′ target site substitution mutants were first tested for transcript cleavage properties using a 5′ RACE assay with transgenic plant extracts. Cleavage at the canonical position of the authentically paired miR390, miR171, and miR159 3′ target sites, but not at the destroyed target site (*35S:TAS3aPDS-3′390mut*), was detected in the majority of cloned 5′ RACE products (Figures 2A and S1A). At miR171 target sites, cleavage offset by three nucleotides from the canonical position was also detected, likely a result of cleavage guided by the distinct miR171b/c isoform (Figures 2A, S1A, and S1B). Cleavage was not detected at the authentic 5′ miR390 target site from any construct or at the destroyed 5′ site, and was rare at predicted noncleavable heterologous 5′ target sites (Figures 2A and S2A) (data not shown). Therefore, the 5′ and 3′ substitution variants generally possessed target site cleavage properties as intended.

The miR171 and miR159 3′ target site substitution and parental constructs triggered photobleaching in 65%–97% of plants (Figures 2A and S1A). Photobleaching was absent in plants with a noncleavable 3′ target-site construct (*35S:TAS3aPDS-3′390mut*; Figure S1A). Syn-tasiRNA levels were not significantly different in Col-0 plants with either the parental *35S:TAS3aPDS-2* or the miR171 3′ target substitution construct (p value = 0.55, two-sample t test), but importantly, photobleaching triggered by both constructs was lost in *zip-1* plants (Figure 2A). This indicated that substitution of the 3′ miR390 target site with a

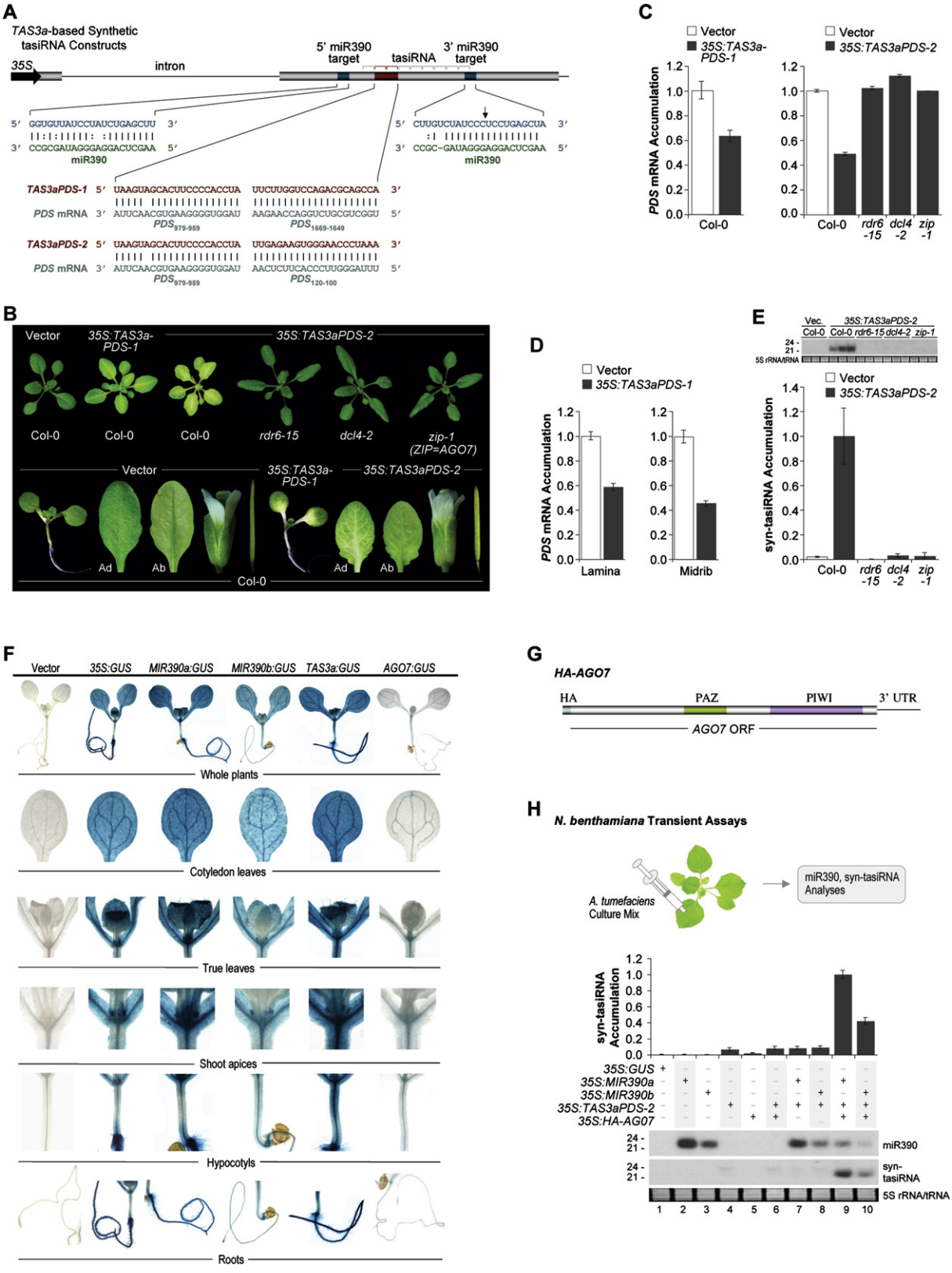
A
TAS3a-based Synthetic tasiRNA Constructs
35S
intron
5' miR390 target
tasiRNA
3' miR390 target
miR390
TAS3aPDS-1
PDS mRNA
TAS3aPDS-2
B
Vector
35S:TAS3a-PDS-1
35S:TAS3aPDS-2
Col-0
rdr6-15
dcl4-2
zip-1 (ZIP=AGO7)
Ad
Ab
C
PDS mRNA Accumulation
D
Lamina
Midrib
E
syn-tasiRNA Accumulation
5S rRNA/tRNA
F
35S:GUS
MIR390a:GUS
MIR390b:GUS
TAS3a:GUS
AGO7:GUS
Whole plants
Cotyledon leaves
True leaves
Shoot apices
Hypocotyls
Roots
G
HA-AGO7
HA
PAZ
PIWI
3' UTR
AGO7 ORF
H
N. benthamiana Transient Assays
A. tumefaciens Culture Mix
miR390, syn-tasiRNA Analyses
35S:MIR390a
35S:MIR390b
35S:HA-AG07
miR390
syn-tasiRNA

functional, alternative target site is tolerated, but does not overcome the system requirement for AGO7.

In contrast to the functional 3′ substitutions, both cleavable (*35S:TAS3aPDS-5′171cle-2* and *35S:TAS3aPDS-5′3′171cle-2*) and noncleavable (*35S:TAS3aPDS-5′171nc-2*) miR171 target substitutions at the 5′ site eliminated photobleaching and reduced syn-tasiRNAs to background levels in Col-0 plants, regardless of the identity of the 3′ target site (Figures 2A and 2B). Each of the other heterologous 5′ target sites, and the destroyed 5′ site, resulted in low or nondetectable syn-tasiRNA levels and loss of photobleaching (Figures S2A and S2B). It is possible that loss of syn-tasiRNA was caused by misprocessing of the transcripts, such that tasiRNAs were formed upstream (5′) of the 5′ target sites. However, we failed to detect small RNAs using probes corresponding to sequences on the 5′ side of any of the modified 5′ target sites (Figure S2B). The collective target-site substitution data indicate requirements for a 5′ miR390 target site (in a noncleaved format [Axtell et al., 2006]) and a functional 3′ cleavage site, though not necessarily a miR390 site.

Table 1. Effects of *TAS3a*-Based Syn-tasiRNA on Wild-Type and Mutant Plants

Genotype	n	Syn-tasiRNA[a]		Relative Photobleaching[b]		
		PDSd7[c]	PDSd8[d]	none	weak	moderate
Col-0						
Vector	90	–	–	100.0	0	0
35S:TAS3aPDS-1	81	+	+	3.5	96.5	0
35S:TAS3aPDS-2	12	+	+	8.3	16.7	75.0
rdr6-15						
35S:TAS3aPDS-1	85	–	–	100.0	0	0
35S:TAS3aPDS-2	36	–	–	100.0	0	0
dcl4-2						
35S:TAS3aPDS-1	5	–	–	100.0	0	0
35S:TAS3aPDS-2	36	–	–	100.0	0	0
zip-1						
35S:TAS3aPDS-1	12	–	–	100.0	0	0
35S:TAS3aPDS-2	36	–	–	100.0	0	0

[a] Syn-tasiRNA are scored as either present (+) or absent (–) as determined by RNA blot assays.
[b] Photobleaching is shown as a percentage of plants in each category.
[c] The PDSd7 (position 5′ D7[+]) syn-tasiRNA differs between each of the syn-tasiRNA constructs.
[d] The PDSd8 (position 5′ D8[+]) syn-tasiRNA is identical in each of the syn-tasiRNA constructs.

Role of AGO7 in *TAS3a* Transcript Processing

To determine if AGO7 is required for cleavage of endogenous *TAS3a* transcripts, 5′ RACE assays were done using wt and mutant plants. 5′ RACE product corresponding to cleavage of *TAS3a* transcript at the 3′ miR390 target site was detected in Col-0 plants (Figure 3A). A slightly larger 5′ RACE product corresponding to cleavage 33 bases upstream of the miR390 cleavage site was also detected (Figure 3A, lanes 1–3). As shown previously (Allen et al., 2005), this product corresponds to cleavage guided by a secondary siRNA (*TAS3a* 5′ D2[–]) derived from the *TAS3a* complementary strand. In *rdr6-15* plants, 5′ RACE product corresponding to cleavage at the 3′ miR390 site, but not at the secondary site, was detected (Figure 3A; lanes 4–6). Loss of secondary cleavage in *rdr6-15* was expected due to lack of the complementary RNA strand from which the secondary siRNA originates. In *zip-1* plants, 5′ RACE products corresponding to both miR390-guided and secondary cleavage events were lost (Figure 3A; lanes 7–9), indicating that AGO7 is necessary for initiation cleavage of endogenous *TAS3a* transcript.

To further explore the connection between AGO7 and miR390-guided cleavage, parental *35S:TAS3aPDS-2* and each single and dual miR171 target-site substitution construct (Figure 2A) was transiently expressed in *N. benthamiana*. When expressed alone or in combination with *35S:MIR171a* and *35S:MIR390a*, each construct failed to yield syn-tasiRNA (Figure 3C; lanes 3–12). But when coexpressed with *35S:MIR171a*, *35S:MIR390a,* and *35S:HA-AGO7*, both the parental construct and the single 3′ miR171 target-site substitution construct yielded relatively high levels of syn-tasiRNA (Figure 3C; lanes 13 and 14). However, none of the single or dual miR171 substitution constructs with a 5′ miR171 target site yielded syn-tasiRNA, even when coexpressed with *35S:HA-AGO7* (Figure 3C; lanes 15–17). Cleavage was detected at each of the 3′ and cleavable 5′ miR171 target sites in the presence and absence of HA-AGO7 (Figure 3D; lanes 3, 5, 6, 8, 10, and 11), indicating that another AGO protein (likely AGO1, see below) functions in association with miR171. Ectopic miR171 was not required for cleavage at miR171 target sites due to relatively high levels of endogenous miR171 (Figure 3D; lanes 3, 5, and 6). In contrast to miR171 target sites, processing at the authentic 3′ miR390 target site was dependent on coexpression with *35S:HA-AGO7*, irrespective of the corresponding 5′ target site (Figure 3D; lanes 7, 9, and 10 versus lanes 12, 14, and 15). The requirements for AGO7 and miR390 in cleavage and syn-tasiRNA formation are summarized in Figure 3E. The requirement of AGO7 for cleavage specifically at the 3′ miR390 target site, but not at miR171 target sites, suggests that AGO7 functions as a miR390-specific slicer.

Figure 1. Functionality and Genetic Requirements of *TAS3a*-Based syn-tasiRNA

(A) Organization of syn-tasiRNA constructs. The miR390-guided cleavage site is indicated by the arrow. The tasiRNA region is indicated by brackets.
(B) Phenotypes of Col-0 and mutant plants containing empty vector, *35S:TAS3aPDS-1*, and *35S:TAS3aPDS-2* (Ad = adaxial, Ab = abaxial).
(C) Mean relative level ± SE of *PDS* mRNA in rosette tissue (Col-0 vector = 1.0).
(D) Mean relative level ± SE of *PDS* mRNA in leaf midrib and lamina tissue (Col-0 vector = 1.0).
(E) Mean relative level ± SE of syn-tasiRNA (Col-0 *35S:TAS3aPDS-2* = 1.0). Inset shows small RNA blot data.
(F) GUS activity in seedlings of Col-0 plants transformed with the indicated constructs.
(G) Organization of *HA-AGO7*.
(H) Mean relative levels ± SE of syn-tasiRNA with blot images for miR390 and syn-tasiRNA from one replicate (*35S:MIR390a* + *35S:TAS3aPDS-2* + *35S:HA-AGO7* = 1.0) from a transient assay in *N. benthamiana*.

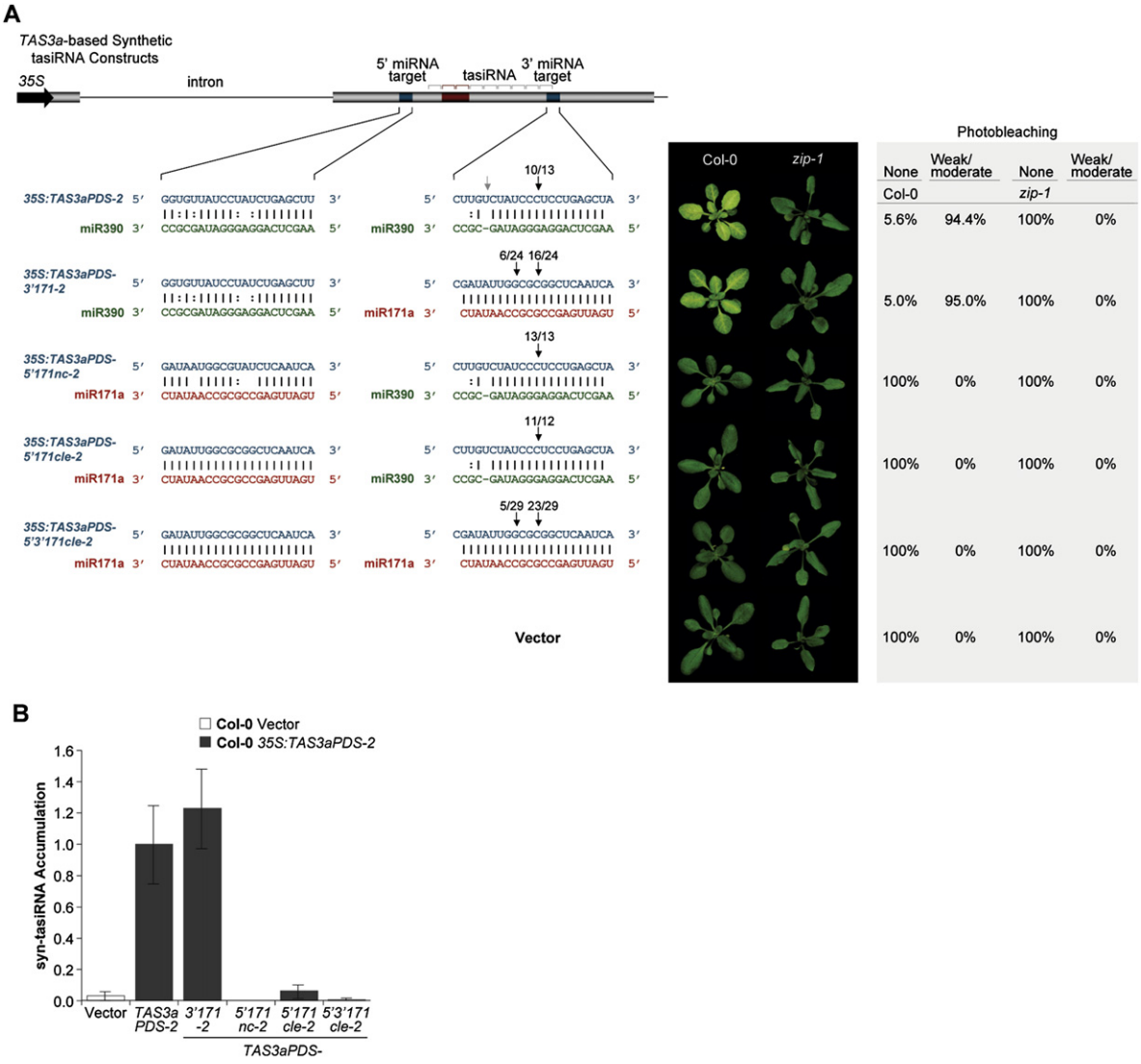

Figure 2. Requirement and Specificity of miR390 for Syn-tasiRNA Formation

(A) The 3′ and/or 5′ miR390 target sites in *35S:TAS3aPDS-2* were substituted for miR171 target sites. The proportion of cloned 5′ RACE products corresponding to cleavage at the canonical position at each target site in Col-0 plants is indicated above the black arrows. 5′ RACE products from noncanonical positions at each target site are indicated by gray arrows, although proportions are not indicated. The percentages of plants that displayed photobleaching are shown next to representative images of rosettes (for each line, n ≥ 5 primary transformants analyzed).

(B) Mean relative level ± SE of syn-tasiRNA (Col-0 *35S:TAS3aPDS-2* = 1.0).

AGO7 Associates Specifically with miR390

To determine if AGO7 associates specifically with miR390, an HA-tagged AGO7 construct (*AGO7:HA-AGO7*) containing authentic 5′ and 3′ regulatory sequences was introduced into Col-0 and *zip-1* plants and analyzed for small RNA association in coimmunoprecipitation (coIP) assays. *zip-1* plants exhibit a number of developmental abnormalities, including defects in leaf development, vegetative timing, and seed set. The *AGO7:HA-AGO7* construct complemented the *zip-1* developmental defects and restored *TAS3* tasiRNA (Figure 4A). Pre-IP (input) and anti-HA IP fractions from extracts of *zip-1* vector- and *AGO7:HA-AGO7*-transformed plants were analyzed for AGO7, miR171, and miR390. HA-AGO7 was detected only in the input and IP fractions from *zip-1* plants with *AGO7:HA-AGO7*. miR171 and miR390 were detected in the input fraction of both *zip-1* vector- and *AGO7:HA-AGO7*-transformed plants, but only miR390 coimmunoprecipitated with HA-AGO7 (Figure 4B). Neither miR171 nor miR390 was detected in the IP fraction from *zip-1* vector-transformed plants (Figure 4B; lane 2).

The AGO7-associated small RNAs were probed more exhaustively by sequencing amplified small RNA populations from HA-AGO7 input and IP fractions (Figure 4B; flow chart). Small RNA of the 24 nt size class were most abundant in the input fraction, whereas 21 nt small RNAs were most abundant in the IP fraction (Figure S3A). Read numbers for previously defined *Arabidopsis* miRNA and tasiRNA families were recorded from

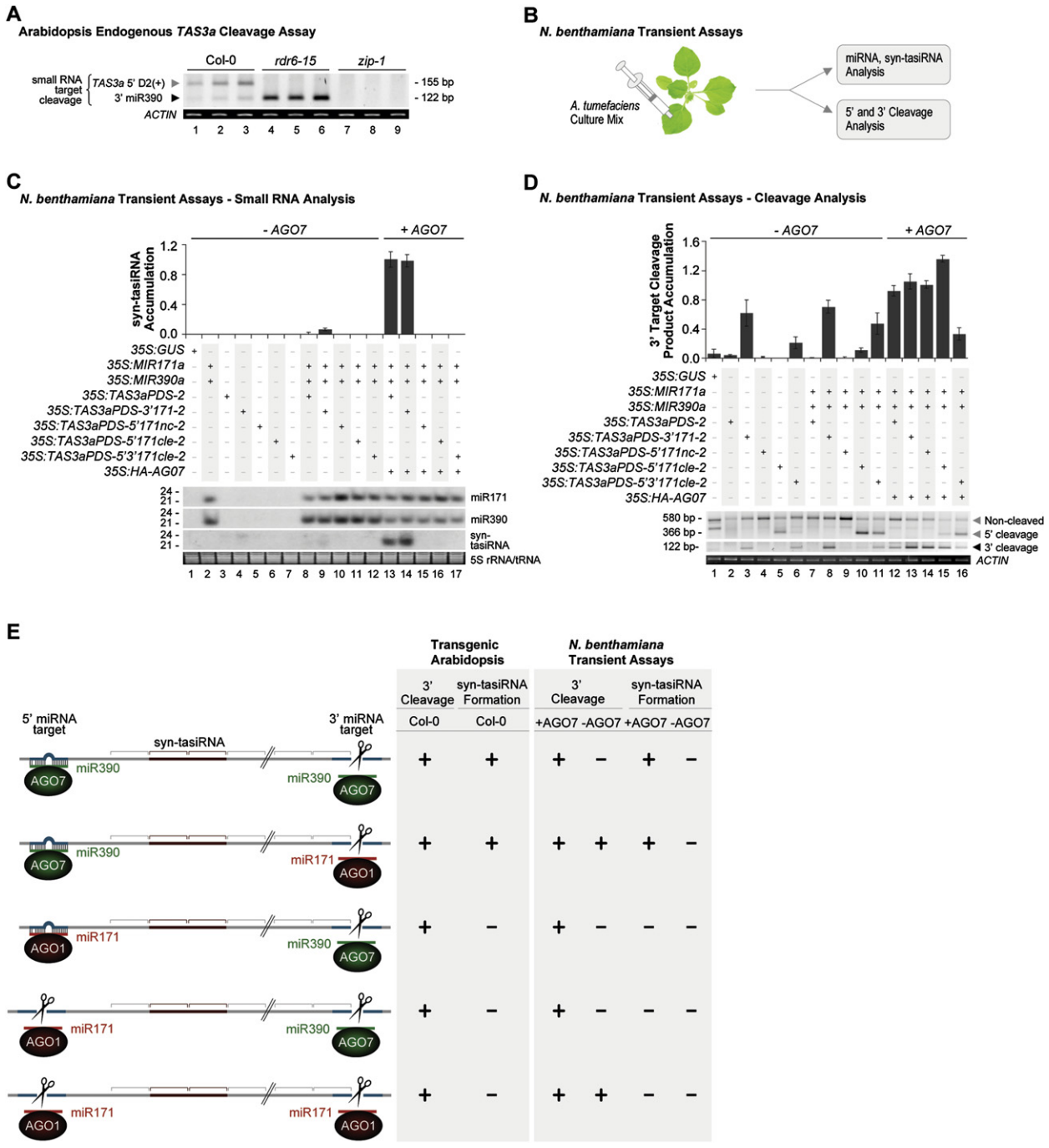

Figure 3. AGO7 and miR390 Requirements for Processing of *TAS3a*-Derived Transcripts

(A) 5′ RACE assay of cleavage of endogenous *TAS3a* transcripts.

(B) Schematic for transient expression assay in *N. benthamiana*.

(C) RNA blot assays for small RNAs, with mean relative levels ± SEs of syn-tasiRNA shown, and blot images shown for one replicate (*35S:MIR171a* + *35S:MIR390a* + *35S:TAS3aPDS-2* + *35S:HA-AGO7* = 1.0).

(D) 5′ RACE assay of miRNA-guided cleavage. Mean relative levels ± SEs of 3′ cleavage product accumulation corresponding to cleavage at the 3′ miRNA target sites, with gel images shown for one replicate (*35S:MIR171a* + *35S:MIR390a* + *35S:TAS3aPDS-2* + *35S:HA-AGO7* = 1.0).

(E) Summary of miR390 and AGO7 requirements for cleavage and syn-tasiRNA formation in modified *TAS3a*-based syn-tasiRNA transcripts.

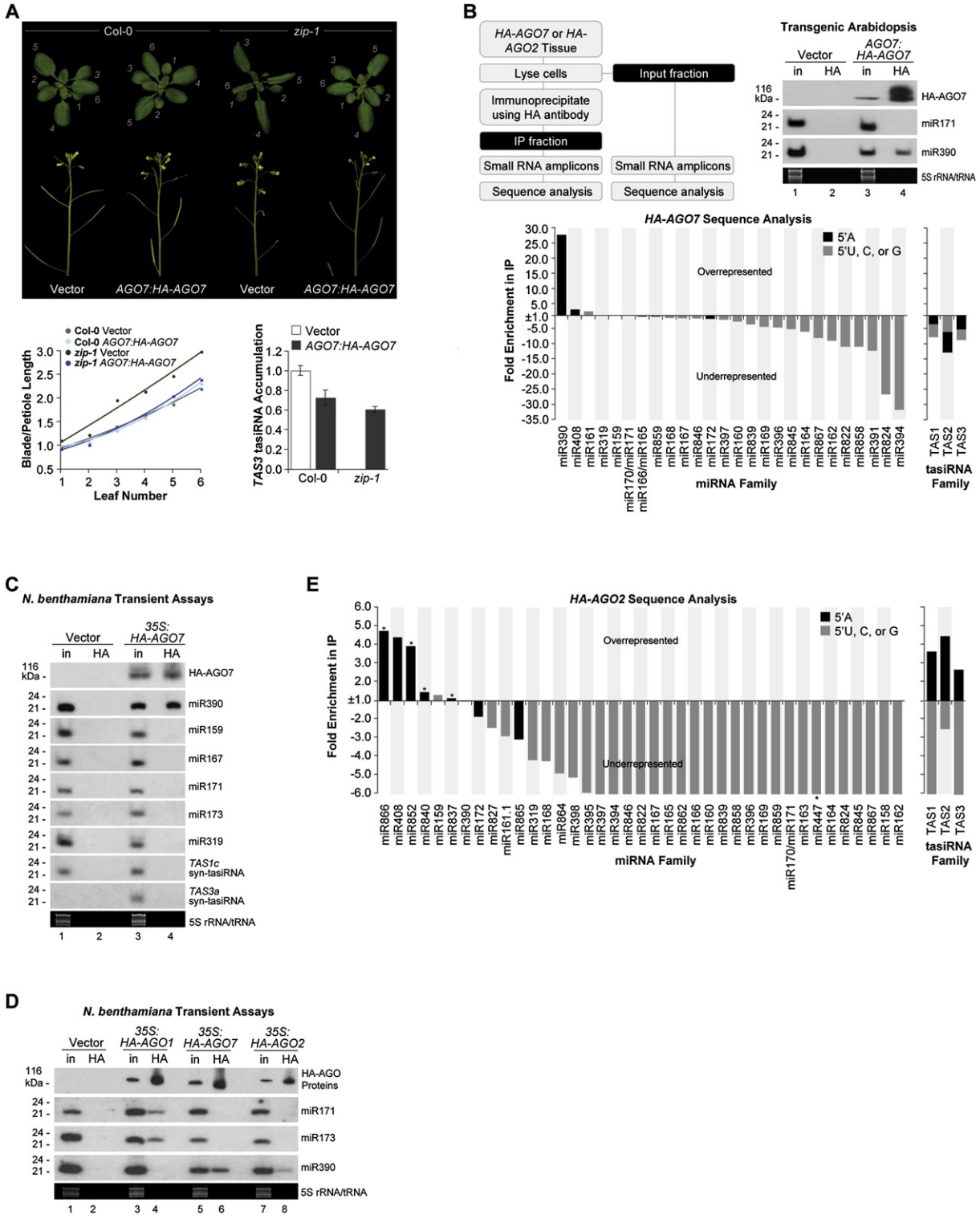

Figure 4. Small RNA Interactions with AGO1, AGO2, and AGO7

(A) Wild-type (Col-0) and *zip-1* vector- and *AGO7:HA-AGO7*-transformed plants. Mean ± SE of leaf blade length/petiole length ratios for leaves 1–6 ($n \geq 17$ for each line) are shown in the line graph. Mean relative levels ± SE of *TAS3a* tasiRNA (Col-0 vector-transformed = 1.0) are shown in the bar graph.

(B) Analysis of *Arabidopsis* small RNA populations associated with HA-AGO7. Protein and RNA blot assays using input (in) and IP (HA) fractions are on the right of the flowchart. Enrichment or depletion of the indicated miRNA and tasiRNA families in the HA-AGO7 IP fraction relative to the input fraction is shown in the lower graph.

the input (10,226) and IP (14,226) fractions (Table S2). Absolute read counts as a reflection of AGO7-associated small RNAs in the IP fraction, however are not directly interpretable due to the effects of contamination with AGO7-non-associated small RNA. For example, reads of a highly enriched, but low-abundance, miRNA could be dwarfed by reads from a normally abundant miRNA that contaminates the IP fraction. Therefore, small RNA association with AGO7 was assessed by calculating enrichment in the IP fraction relative to the input fraction. Overall representation of individual family reads/total miRNA+tasiRNA reads in IP and input fractions was determined for each family, and enrichment or depletion in the IP fraction was calculated using the IP representation/input representation ratio. Only miRNA or tasiRNA families that were represented in both input and IP fractions, and by at least five reads in either fraction, were included in the analysis. miR390 and miR391, which comprise one miRNA family, were treated independently here because of their specific relevance to the *TAS3* pathway.

The majority of miRNA families were underrepresented in the IP fraction (Figure 4B). Similarly, each of three tasiRNA families were underrepresented. In contrast, miR390 was enriched ~28-fold in the IP fraction. miR390 was the only miRNA enriched more than 3.1-fold (Figure 4B), suggesting that AGO7 has a unique affinity for miR390. Interestingly, miR391 was underrepresented in the IP fraction. Also, several miRNA families were neither enriched nor depleted in the IP fraction. While this could conceivably reflect a weak or unstable association with AGO7, the high endogenous levels for most of these families suggests it is more likely due to nonspecific contamination.

The apparent preference of AGO7 for miR390 in *Arabidopsis* plants could be explained by a unique overlap in expression domains of *AGO7* and *MIR390* genes. To eliminate confounding spatial and temporal effects, competition IP assays were done using the transient expression system. In three of four assays, *35S:HA-AGO7* or empty vector was coexpressed with *35S:TAS3aPDS-2, 35S:MIR390a* and one or two additional 35S promoter-driven *MIRNA* constructs (for miR171, miR159, miR167, and miR319). In a fourth assay, *35S:HA-AGO7* or empty vector was coexpressed with *35S:MIR390a*, *35S:TAS3aPDS-2*, *35S:MIR173a*, and a 35S-driven *TAS1c*-based synthetic tasiRNA construct (*35S:TAS1cPDS-2*). miR390 coimmunoprecipitated with HA-AGO7 in each of the competition assays (Figure 4C, lane 4; only one experiment). In contrast, none of the other miRNAs or syn-tasiRNAs tested coimmunoprecipitated with HA-AGO7 (Figure 4C; lane 4), strongly supporting the hypothesis that AGO7 associates specifically with miR390.

miR390 Selectivity for AGO7

The association of AGO7 with miR390 led to the question of whether or not miR390 is excluded from the other *Arabidopsis* AGO proteins that associate with miRNAs. HA-AGO1 and HA-AGO2 were compared to HA-AGO7 for their association with miR390, miR171, and miR173 in competition IP assays. AGO1 is known to associate with most miRNAs, *TAS1* tasiRNA, and some viral siRNA (Baumberger and Baulcombe, 2005; Qi et al., 2005, 2006; Zhang et al., 2006). Little is known about AGO2 functionality, but it was chosen because of close relatedness to AGO7 within the 10-member AGO family in *Arabidopsis* (Tolia and Joshua-Tor, 2007). *35S:HA-AGO1, 35S:HA-AGO2, 35S:HA-AGO7*, or empty vector was coexpressed with *35S:MIR171a* alone or a mixture of *35S:MIR173a* and *35S:MIR390a*. Consistent with previous experiments, only miR390 coimmunoprecipitated with AGO7 (Figure 4D; lanes 5 and 6). Conversely, miR171 and miR173, but not miR390, coimmunoprecipitated with AGO1 (Figure 4D; lanes 3 and 4), indicating reciprocal specificity between AGO7 and AGO1 for the miRNAs tested. miR390 coimmunoprecipitated with AGO2, but at a relatively low level, while miR171 and miR173 did not (Figure 4D; lanes 7 and 8). Using transgenic Col-0 plants expressing HA-AGO2 from authentic regulatory signals (*AGO2:HA-AGO2*), small RNAs associated with AGO2 were sequenced, and enrichment/depletion ratios were calculated. Small RNAs in the HA-AGO2 IP fraction were primarily 21 nt in length (Figure S3B). Most miRNAs and tasiRNAs were depleted in the HA-AGO2 IP fraction, but with a few notable exceptions. Six miRNAs were moderately or slightly enriched (Figure 4E; Table S3). Although the miR390 ratio was neutral, it ranked seventh among miRNA families. Interestingly, six of the top seven ranking miRNAs, including miR390, contain 5′A residues, which contrasts with the vast majority of miRNAs, including miR171 and miR173, which contain 5′U. Additionally, the 5′A-containing subset of tasiRNAs from three families were specifically enriched by HA-AGO2 IP, whereas non-5′A-containing tasiRNAs were depleted. These results hint at a prospective 5′ rule for specificity of AGO1 and AGO2, in which they interact preferentially with 21 nt small RNAs containing 5′U or 5′A, respectively. AGO7 specificity for miR390, however, may have more complex requirements than can be explained by a simple 5′ feature.

Specificity in AGO7-miR390 Complex Formation and 5′ Nucleotide Discrimination

To test directly the miR390 5′ nucleotide requirement, as well as the roles of additional features of the *MIR390a* foldback, in AGO7 loading specificity, mutant and chimeric miR390- and miR171-expressing constructs were analyzed (Figure 5A). As described above, these experiments were done in the context of AGO1, AGO2, and AGO7 proteins to understand both the AGO7-miR390-specific features and the broader principles of AGO-miRNA complex formation.

We first hypothesized that the strong association of miR390 with AGO7 is dictated by the miR390 5′A. We also hypothesized

(C) Protein and RNA blot assays using input (in) and IP (HA) fractions from *N. benthamiana* following coexpression of empty vector or *35S:HA-AGO7* and *35S:TAS3aPDS-2* or *35S:TAS1cPDS-2,* and various 35S-promoter driven *MIRNA* constructs.

(D) Protein and RNA blot assays using input (in) and IP (HA) fractions from *N. benthamiana* following coexpression of empty vector, *35S:HA-AGO1, 35S:HA-AGO7*, or *35S:HA-AGO2* and various 35S-promoter-driven *MIRNA* constructs.

(E) Enrichment or depletion of the indicated miRNA and tasiRNA families in the *Arabidopsis* HA-AGO2 IP fraction relative to the input fraction. Underrepresentation ranged from −1.1- to −255-fold, but the display was limited at −6.0. Families for which no reads were obtained from one fraction, but for which at least 14 reads were obtained in the other fraction, are marked with an asterisk.

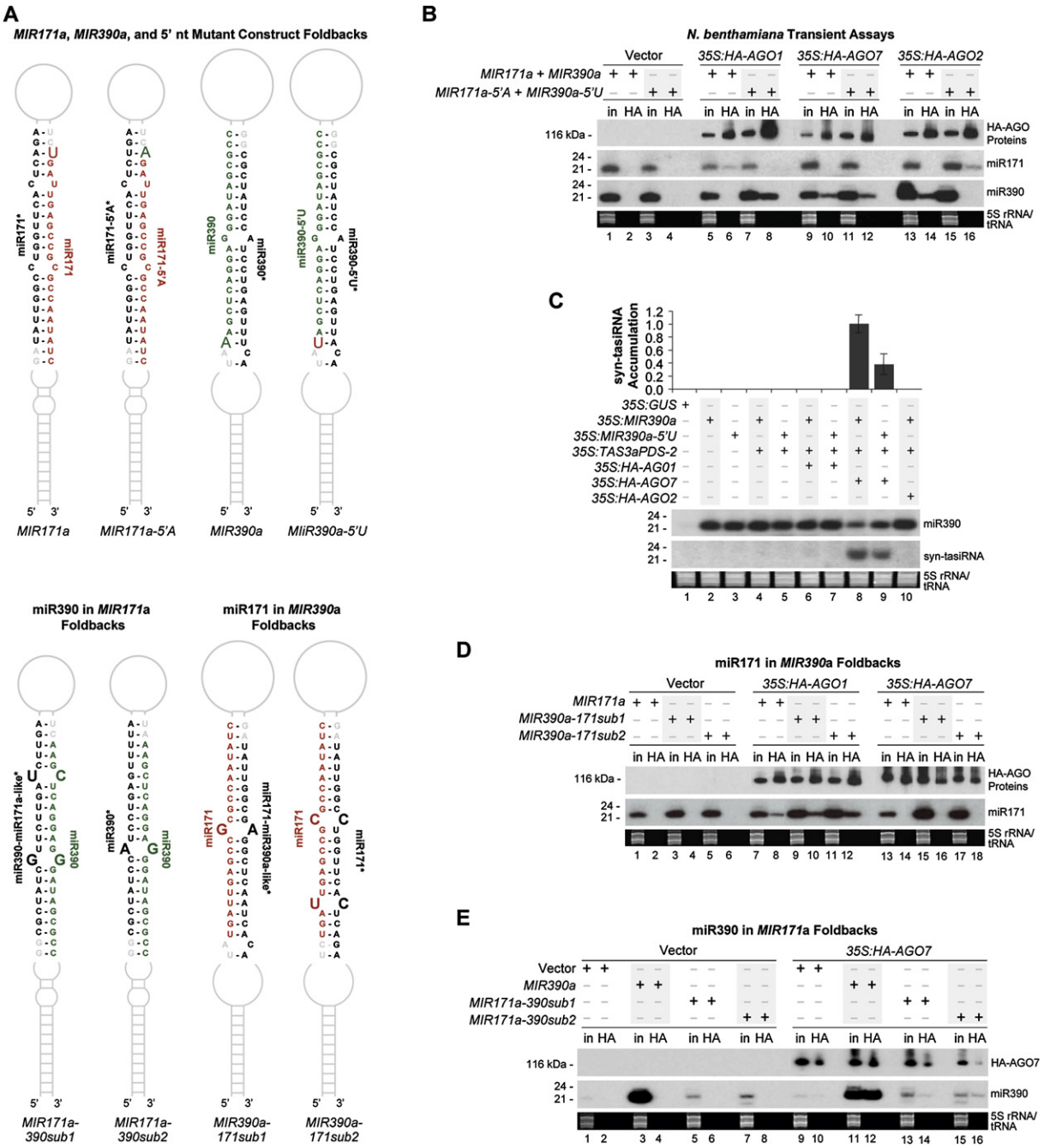

Figure 5. Specificity Determinants for AGO1, AGO2, and AGO7

(A) Predicted foldbacks of *MIR171a* and *MIR390a* mutant and chimeric constructs.

(B) Protein and RNA blot assays using input (in) and IP (HA) fractions from *N. benthamiana* following coexpression of empty vector, *35S:HA-AGO1*, *35S:HA-AGO7*, or *35S:HA-AGO2* and 35S-promoter-driven parental or mutant *MIR171a* and *MIR390a* constructs.

(C) RNA blot assays for miR390 and syn-tasiRNA from *N. benthamiana* assays. Mean relative levels ± SE of syn-tasiRNA are shown with blot images for one replicate (*35S:MIR390a* + *35S:TAS3aPDS-2* + *35S:HA-AGO7* = 1.0).

(D and E) Protein and RNA blot assays using input (in) and IP (HA) fractions of leaf tissue extracts from *N. benthamiana* following coexpression of empty vector, *35S:HA-AGO1*, or *35S:HA-AGO7* and 35S-promoter-driven *MIR171a*, *MIR390a*, or *MIR171a/MIR390a* chimeric constructs.

that miR171 associates with AGO1 due to a 5′U. Parental *35S:MIR171a* and *35S:MIR390a* were mutated to convert the 5′ nucleotides of miR171 and miR390 to A and U (forming *35S:MIR171a-5′A* and *35S:MIR390a-5′U*), respectively, and miRNA association with HA-tagged AGO1, AGO2, and AGO7 was assessed in coIP assays (Figure 5A). HA-AGO1 specifically

coimmunoprecipitated with each 5′U-containing miRNA (miR171 and miR390-5′U), but not with 5′A-containing miRNAs (miR390 and miR171-5′A) (Figure 5B). In the reciprocal pattern, HA-AGO2 specifically coimmunoprecipitated with 5′A-containing miRNAs (miR390 and miR171-5′A), but not with either miRNA containing a 5′U (miR171 and miR390-5′U) (Figure 5B). These data reveal the 5′ nucleotide as a simple specificity determinant for inclusion/exclusion from AGO1 (5′U) and AGO2 (5′A) complexes. However, loading of AGO1 with miR390-5′U, or AGO2 with miR390, in the absence of AGO7 was insufficient to trigger syn-tasiRNA formation in coexpression assays with *35S:TAS3aPDS-2* (Figure 5C; lanes 7 and 10).

In sharp contrast, HA-AGO7 coimmunoprecipitated with miR390 containing either a 5′A or 5′U, and failed to associate with either miR171 or miR171-5′A (Figure 5B). Coexpression of either *35S:MIR390a-5′U* or *35S:MIR390a* with *35S:HA-AGO7* and *35S:TAS3aPDS-2* triggered syn-tasiRNA formation, although syn-tasiRNA levels were lower in the assay containing *35S:MIR390a-5′U* (Figure 5C; lanes 8 and 9). AGO7, therefore, neither loads miR390 on the basis of a 5′A nor excludes miR171 due to a 5′U, and the 5′ identity has only modest effects on functionality of miR390-AGO7 complexes during tasiRNA biogenesis.

Finally, to determine if the *MIR390a* foldback contains unique sequence or structural features for loading miR390 into AGO7, chimeric *MIR171a* and *MIR390a* constructs were tested in coIP assays with HA-AGO1 and HA-AGO7. In the first series, two miR171 duplex forms, one with an authentic miR171 duplex-mispair structure (C:C and U:C mispairs, *35S:MIR390a-171sub2*) and the other with a miR390-like duplex mispair structure (single G:A mispair, *35S:MIR390a-171sub1*), were introduced into the *MIR390a* precursor in place of the miR390 duplex (Figure 5A). miR171 expressed from these chimeric constructs accumulated to higher levels than when derived from the authentic *MIR171a* context, but coimmunoprecipitated specifically with HA-AGO1 regardless of the precursor context (Figure 5D; lanes 7–12). None of the chimeric miR171-generating precursors yielded miR171 with the capacity to coIP with HA-AGO7 (Figure 5D; lanes 13–18), indicating that neither the *MIR390a* precursor stem-loop backbone, nor the positions of mispairs within the *MIR390a* miRNA-miRNA* duplex, are sufficient to direct association with AGO7. In the second series, two miR390a duplex forms, one with an authentic miR390 duplex-mispair structure (G:A mispair, *35S:MIR171a-390sub2*) and the other with an miR171-like duplex mispair structure (G:G and C:U mispairs, *35S:MIR171a-390sub1*), were introduced into the *MIR171a* precursor in place of the miR171 duplex (Figure 5A). miR390 was only weakly expressed from the chimeric *MIR171a*-based constructs, although miR390 levels from both constructs were above the low endogenous miR390 levels (2.8- to 4.1-fold; Figure 5E, lanes 9, 13, and 15). miR390 derived from the authentic miR390 precursor, as well as from both of the chimeric *MIR171a*-based constructs, coimmunoprecipitated with HA-AGO7 (Figure 5E; lanes 11–16), but not with HA-AGO1 (data not shown). These results indicate that selective association of AGO7 with miR390 cannot be explained by a 5′ nucleotide rule or a foldback-related structure, but rather point to a specific non-5′ nucleotide feature of the miR390 sequence itself.

DISCUSSION

Using the syn-tasiRNA system, we identified mechanistic features by which two miR390 target sites function specifically with AGO7 to route *TAS3* transcripts through the RDR6/DCL4 pathway. Cleavage at the 3′ target site of *TAS3a*-derived transcripts forms the 3′ end at which RDR6 initiates transcription, synthesizing a dsRNA substrate for subsequent processing by DCL4. Cleavage at the 3′ miR390 target site requires AGO7, irrespective of targeting at the 5′ site, suggesting that AGO7 functions as a miR390-guided slicer. The requirement for AGO7 slicer function is bypassed when the 3′ miR390 target site is substituted for heterologous miRNA target sites, indicating that AGO7 is dispensable at this site if another AGO is delivered via an alternate miRNA guide. The obvious prediction from this result, that AGO7 is uniquely associated with miR390, was confirmed in multiple coIP assays. Therefore, the functionality of AGO7 at the 3′ target site is dictated entirely by its miR390-guided slicer activity.

The *TAS3a* 5′ miR390 target-site duplex contains requisite mispairs that interfere with cleavage (Axtell et al., 2006). However, this site is clearly active, and in contrast to the 3′ target site, the 5′ site is far less tolerant of target-site substitutions. The dependence on a 5′ miR390 target site may reflect several possible requirements. There may be a requirement for a miR390 guide and/or miR390 target sequence per se, although the unique contribution of the nucleotide sequences themselves is not obvious. Furthermore, AGO1-miR390-5′U complexes failed to trigger tasiRNA formation, suggesting that there is a unique requirement for an AGO7-containing complex at the 5′ target site. The preference for a 5′ miR390 site, therefore, is likely due to a requirement for interaction of an AGO7-miR390 complex with the precursor transcript. Given that the 5′ site functions in a noncleavage mode, the AGO7-miR390 complex is proposed to operate through a "stable" interaction.

How might stable association with an AGO7-miR390 complex facilitate routing of *TAS3a* transcripts through the RDR6/DCL4 pathway? One simple model states that AGO7 stabilizes the processed *TAS3* transcript and provides greater opportunity for interaction with RDR6 (Figure 6A). Alternatively, AGO7 may actively recruit RDR6 through direct interaction or through associated factors, such as SGS3 (Figure 6A). In *Arabidopsis*, AGO4 interacts with NRPD1b, a subunit of PolIVb (Li et al., 2006; El-Shami et al., 2007), so there is precedence for AGO proteins interacting with a polymerase-like protein. A 3′ end formed by small RNA-directed cleavage or by other cleavage mechanisms may be a preferred end for RDR6 activity, possibly due to loss of the poly(A) tail and associated factors. As another possibility, stable association of AGO7 might physically direct transcripts into an RDR6/DCL4-containing processing center (Figure 6A). Although an RDR6/DCL4 processing center has not been identified, RNA-processing centers with roles in silencing, such as P bodies (Liu et al., 2005), have been identified.

Most miRNA target transcripts are not routed through the RDR6/DCL4 pathway (Axtell et al., 2006; Howell et al., 2007; Lu et al., 2006; Ronemus et al., 2006), and this may relate to rapid dissociation of the AGO-containing complex after cleavage interaction at single sites. Among the relatively few targets that feed into the RDR6/DCL4 pathway are several transcripts encoding pentatricopeptide repeat (PPR) proteins (Axtell et al.,

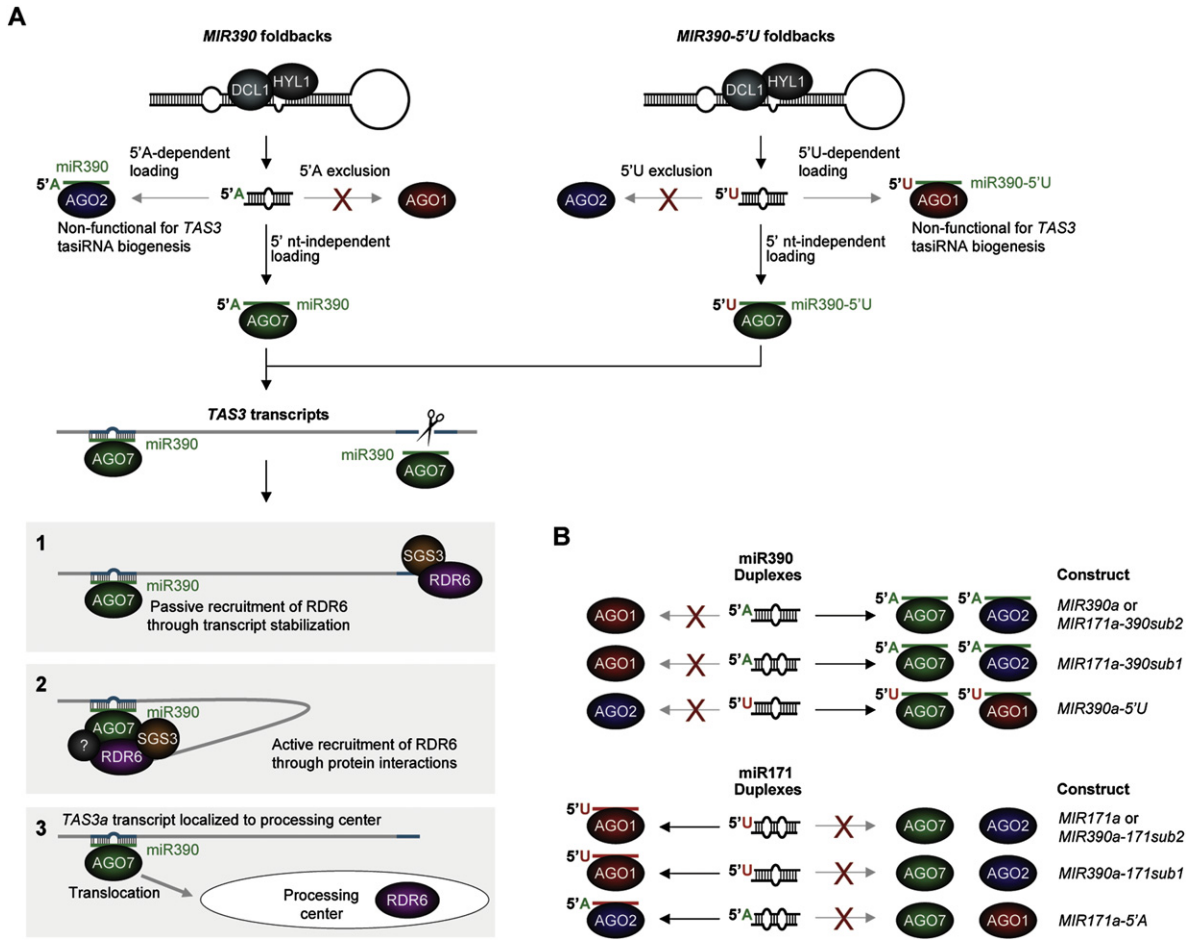

Figure 6. miR390-AGO Specificity and Three Models for Recruitment of RDR6 to *TAS3* Transcripts

(A) 5′ nucleotide specificity rules apply to AGO1 and AGO2, but not AGO7. Three models (1–3) to explain how the 5′ miR390-AGO7 complex recruits RDR6 to *TAS3* transcripts are shown in the shaded boxes.

(B) Summary of AGO specificity for miRNA derived from each of the *MIR171a* and *MIR390a* 5′ nt substitution and chimeric constructs (Figure 5A).

2006; Chen et al., 2007; Howell et al., 2007; Lu et al., 2006). Notably, these are targeted for cleavage by miR161 isoforms and *TAS1*/*TAS2*-derived tasiRNAs, but are also predicted to be targeted by miR400 (Howell et al., 2007; Peragine et al., 2004; Sunkar and Zhu, 2004). miR400 fails to direct cleavage (Howell et al., 2007) and may associate stably with *PPR* target transcripts. Thus, the combination of small RNA-directed cleavage and noncleaving AGO-containing complexes on a transcript may provide key signals or structures to efficiently recruit RDR6.

Why is AGO1, which will associate with functional miR390-5′U, unable to substitute for AGO7 at the 5′ target site? Perhaps AGO1 fails to recognize or associate stably with more highly mispaired target sites, whereas AGO7 may be more accommodating of miRNA target mispairs. Alternatively, AGO1 may lack an AGO7-like ability to efficiently recruit RDR6 to target transcripts. The known role of AGO1 in RDR6-dependent transgene silencing (Fagard et al., 2000) argues against this idea, although AGO1 may only be necessary for activity (not biogenesis) of secondary siRNA. This idea is weakened further by the fact that *TAS1* and *TAS2* tasiRNA formation requires RDR6 but not AGO7. It will be important to learn if other miRNAs involved in tasiRNA initiation cleavage, such as miR173 and miR828, have unique AGO associations that facilitate routing through the RDR6 pathway.

How did the specialized interaction between AGO7 and miR390 in *TAS3* tasiRNA formation arise? Given the antiquity of the *TAS3* pathway, it is likely that AGO7 has been finely tuned through hundreds of millions of years of evolution to recognize miR390 and exclude other miRNAs. We suggest that AGO7 has subfunctionalized at both the biochemical and expression levels, the result being only a few miRNA target transcripts ushered into the RDR6/DCL4 pathway by AGO7. Similarly, miR390 adopted a 5′A feature that excludes association with AGO1. This 5′ nucleotide exclusion mechanism should limit miR390 activity outside of the AGO7 expression domain. Given the widespread activity of AGO1 as an effector protein for many posttranscriptional silencing pathways, and the apparent broad expression domain of *MIR390a* and *MIR390b*, the 5′ nucleotide exclusion mechanism should focus miR390 activity to cells that coexpress AGO7. We recognize that, despite the

unique affinity of AGO7 for miR390, and the exclusion of miR390 from AGO1, miR390 also associates weakly with AGO2, as well as with AGO4 (Qi et al., 2006). The functional significance of either AGO2 or AGO4 interaction is not understood. Association of miR390 with AGO2 is clearly driven by the 5′A, but the basis for association with AGO4, which interacts primarily with 24 nt siRNA (Qi et al., 2006), is not known. The phenotype of AGO4 mutants does not overlap the phenotype of *TAS3* tasiRNA-deficient mutants (Zilberman et al., 2003). Additionally, AGO7-, *TAS3*-, and RDR6-deficient mutants have similar developmental defects (Adenot et al., 2006; Hunter et al., 2003; Peragine et al., 2004), indicating that neither AGO2 nor AGO4 functions redundantly with AGO7.

Although we could not identify a role for the miRNA 5′ nucleotide as an AGO7 specificity determinant, the 5′ nucleotide was clearly defined as an inclusion/exclusion specificity determinant for both AGO1 and AGO2. AGO1 prefers a 5′U and excludes a 5′A, whereas AGO2 possesses the reciprocal preference for 5′A and exclusion of 5′U. Thus, the selective pressure for a 5′U in the majority of plant miRNAs, which as a class function broadly through AGO1, is now understood. Given the widespread presence of 5′U in animal miRNA, as well as 5′U or other 5′ nucleotide preferences in other small RNA classes (Ruby et al., 2006), similar AGO selectivity determinants very likely explain at least some observed 5′ nucleotide biases more widely. Structural studies show that AGO-siRNA 5′ end interactions are important for recognition, stability, and fidelity of an active effector complex (Ma et al., 2005; Rivas et al., 2005). Indeed, the 5′ terminal base interacts directly through base-stacking interactions with residues in a highly conserved 5′ nucleotide-binding pocket (Ma et al., 2005; Parker et al., 2005). In *Archaeglobus fulgidus* Piwi protein, mutation of a tyrosine residue within the 5′ nucleotide-binding pocket known to interact with the 5′ base results in decreased siRNA-binding affinity (Ma et al., 2005). Thus, it is possible that variation within this pocket accounts for differing 5′ nucleotide specificities among AGO1, AGO2, and AGO7.

Analysis of the chimeric foldbacks indicated that neither the *MIR390a* stem-loop context nor the miR390/miR390* base-pair and mispair features account for the affinity of AGO7 for miR390 (Figure 6B). However, small RNA duplex structure does specify loading for Ago1 and Ago2 in *Drosophila*. miRNAs with central mispairs in the miRNA/miRNA* duplex are preferentially loaded into Ago1, whereas perfectly paired siRNA duplexes are preferentially loaded into Ago2 (Forstemann et al., 2007; Tomari et al., 2007). A similar sorting mechanism exists in *C. elegans* (Steiner et al., 2007). Thus, AGO specificity can be directed by specific 5′ nucleotide identities as well as base-pair structure of precursors. The finding that miR390-AGO7 association depends on additional features suggests there are more specificity determinants to discover.

Finally, the apparent restricted domain of AGO7 promoter activity in *Arabidopsis* plants and the ability of ectopic AGO7 to overcome limitations to syn-tasiRNA formation in *N. benthamiana* leaves suggest that AGO7 may limit activity of the *TAS3* tasiRNA pathway. Interestingly, the syn-tasiRNA-induced photobleaching phenotype appears to emanate from tissue with AGO7 promoter activity. Expansion of the phenotype away from vascular cells may reflect cell-non-autonomy of syn-tasiRNAs. Given that DCL4 products likely function as mobile silencing signals (Dunoyer et al., 2005), *TAS3a*-derived tasiRNAs might function in a cell-non-autonomous manner during plant growth and development.

EXPERIMENTAL PROCEDURES

Transgenes

Transgene sequences were PCR-amplified from genomic DNA or cDNA (Supplemental Experimental Procedures). Syn-tasiRNA sequences, miRNA target-site substitutions, and miR171 and miR390 substitutions were introduced by site-overlap extension PCR (Ho et al., 1989). The resulting products were cloned in pENTR (Invitrogen), followed by recombination into the plant transformation vector pMDC32, pMDC163 (a GUS fusion vector), or pMDC99 (Curtis and Grossniklaus, 2003).

Plant Materials

rdr6-15, dcl4-2, and *zip-1* alleles were previously described (Allen et al., 2004; Hunter et al., 2003; Xie et al., 2005). *Arabidopsis* plants were transformed using *Agrobacterium tumefaciens* GV3101 (Clough and Bent, 1998). Transgenic plants were grown on MS medium containing hygromycin (50 μg/ml) for 7 days, transferred to soil, and maintained in a standard greenhouse with a 16 hr light/8 hr dark supplemental light cycle.

RNA Blots, Quantitative PCR, and 5′ RACE Assays

RNA blot assays were done as described (Allen et al., 2005). Except where noted, triplicate samples from pools of independent primary transformants were analyzed. Quantitative RT-PCR was done using the same RNA preparations used for RNA blots. *PDS* mRNA levels were normalized against *ACTIN2* mRNA levels. miRNA-guided cleavage was tested using RNA ligase-mediated 5′ RACE (Llave et al., 2002) (Supplemental Experimental Procedures).

Transient Expression Assays

Agrobacterium-mediated transient assays in *N. benthamiana* leaves were done as described (Llave et al., 2002). Within each experiment, concentrations of *Agrobacterium* containing each construct were equalized by adjusting the concentration of *Agrobacterium* culture containing empty vector. RNA was analyzed 48 hr postinfiltration.

GUS Assays

Plants were infiltrated with 100 mM sodium phosphate (pH 7), 1 mM potassium ferricyanide, 1 mM potassium ferrocyanide, 16 mM EDTA, 20% methanol, and 1 mg/ml X-glucuronic acid, followed by incubation at 37°C for 3 or 6 hr. Tissue was cleared in ethanol and photographed with an Olympus SZX12 microscope.

Immunoprecipitation

Immunoprecipitation and subsequent RNA isolation were done using HA antibody (clone 12CA5, Roche) (Chapman et al., 2004). For immunoprecipitation from *Arabidopsis* tissue, flower stages 1–12 were used.

Small RNA Sequencing

Flower tissue (stages 1–12) from *zip-1 AGO7:HA-AGO7*- or Col-0 *AGO2:HA-AGO2*-transformed plants was ground in lysis buffer (Chapman et al., 2004). Cell debris was removed by centrifugation for 10 min at 12,000 g, and the supernatant was partitioned into input and IP fractions. RNA was isolated immediately from the input fraction by phenol/chloroform extraction, followed by ethanol precipitation. HA-AGO7 and HA-AGO2 were immunoprecipitated using HA antibody and Protein A agarose beads. After removal of an aliquot, beads were treated with proteinase K. RNA was isolated from the supernatant, and amplicons for sequencing were prepared as described (Kasschau et al., 2007) with the exception of the adaptor sequences and the use of Phusion High-Fidelity DNA Polymerase (Finnzymes). Sequencing by synthesis was done using an Illumina 1G Genome Analyzer.

Statistical Analysis

Statistical analyses were done using S-PLUS (Insightful) and Excel (Microsoft). For multiple comparisons, Bonferroni adjustments were applied to p value significance level cutoffs.

SUPPLEMENTAL DATA

Supplemental Data include three figures, three tables, Supplemental Results, Supplemental Experimental Procedures, and Supplemental References and can be found with this article online at http://www.cell.com/cgi/content/full/133/1/128/DC1/.

ACKNOWLEDGMENTS

We thank Bobby Babra, Desiree Boltz, and Amy Shatswell for technical assistance; Chris Sullivan, Scott Givan and Zach Miller for computational assistance; Kristin Kasschau and Mark Dasenko for assistance with sequencing; and Jim Roberts for stimulating discussions. This work was supported by grants from NSF (MCB-0618433), NIH (AI43288), USDA-NRI (2006-35301-17420), NSFC (30325001), and the Monsanto Corporation.

Received: September 5, 2007
Revised: December 21, 2007
Accepted: February 20, 2008
Published online: March 13, 2008

REFERENCES

Adenot, X., Elmayan, T., Lauressergues, D., Boutet, S., Bouche, N., Gasciolli, V., and Vaucheret, H. (2006). DRB4-dependent TAS3 trans-acting siRNAs control leaf morphology through AGO7. Curr. Biol. *16*, 927–932.

Allen, E., Xie, Z., Gustafson, A.M., Sung, G.H., Spatafora, J.W., and Carrington, J.C. (2004). Evolution of microRNA genes by inverted duplication of target gene sequences in *Arabidopsis thaliana*. Nat. Genet. *36*, 1282–1290.

Allen, E., Xie, Z., Gustafson, A.M., and Carrington, J.C. (2005). microRNA-directed phasing during trans-acting siRNA biogenesis in plants. Cell *121*, 207–221.

Axtell, M.J., Jan, C., Rajagopalan, R., and Bartel, D.P. (2006). A two-hit trigger for siRNA biogenesis in plants. Cell *127*, 565–577.

Axtell, M.J., Snyder, J.A., and Bartel, D.P. (2007). Common functions for diverse small RNAs of land plants. Plant Cell *19*, 1750–1769.

Baumberger, N., and Baulcombe, D.C. (2005). *Arabidopsis* ARGONAUTE1 is an RNA slicer that selectively recruits microRNAs and short interfering RNAs. Proc. Natl. Acad. Sci. USA *102*, 11928–11933.

Chapman, E.J., and Carrington, J.C. (2007). Specialization and evolution of endogenous small RNA pathways. Nat. Rev. Genet. *8*, 884–896.

Chapman, E.J., Prokhnevsky, A.I., Gopinath, K., Dolja, V.V., and Carrington, J.C. (2004). Viral RNA silencing suppressors inhibit the microRNA pathway at an intermediate step. Genes Dev. *18*, 1179–1186.

Chen, H.M., Li, Y.H., and Wu, S.H. (2007). Bioinformatic prediction and experimental validation of a microRNA-directed tandem trans-acting siRNA cascade in Arabidopsis. Proc. Natl. Acad. Sci. USA *104*, 3318–3323.

Clough, S.J., and Bent, A.F. (1998). Floral dip: a simplified method for *Agrobacterium*-mediated transformation of *Arabidopsis thaliana*. Plant J. *16*, 735–743.

Curtis, M.D., and Grossniklaus, U. (2003). A gateway cloning vector set for high-throughput functional analysis of genes in planta. Plant Physiol. *133*, 462–469.

Dunoyer, P., Himber, C., and Voinnet, O. (2005). DICER-LIKE 4 is required for RNA interference and produces the 21-nucleotide small interfering RNA component of the plant cell-to-cell silencing signal. Nat. Genet. *37*, 1356–1360.

El-Shami, M., Pontier, D., Lahmy, S., Braun, L., Picart, C., Vega, D., Hakimi, M.A., Jacobsen, S.E., Cooke, R., and Lagrange, T. (2007). Reiterated WG/GW motifs form functionally and evolutionarily conserved ARGONAUTE-binding platforms in RNAi-related components. Genes Dev. *21*, 2539–2544.

Fagard, M., Boutet, S., Morel, J.B., Bellini, C., and Vaucheret, H. (2000). AGO1, QDE-2, and RDE-1 are related proteins required for post-transcriptional gene silencing in plants, quelling in fungi, and RNA interference in animals. Proc. Natl. Acad. Sci. USA *97*, 11650–11654.

Fahlgren, N., Montgomery, T.A., Howell, M.D., Allen, E., Dvorak, S.K., Alexander, A.L., and Carrington, J.C. (2006). Regulation of AUXIN RESPONSE FACTOR3 by TAS3 ta-siRNA affects developmental timing and patterning in Arabidopsis. Curr. Biol. *16*, 939–944.

Forstemann, K., Horwich, M.D., Wee, L., Tomari, Y., and Zamore, P.D. (2007). Drosophila microRNAs are sorted into functionally distinct Argonaute complexes after production by Dicer-1. Cell *130*, 287–297.

Garcia, D., Collier, S.A., Byrne, M.E., and Martienssen, R.A. (2006). Specification of leaf polarity in Arabidopsis via the trans-acting siRNA pathway. Curr. Biol. *16*, 933–938.

Gasciolli, V., Mallory, A.C., Bartel, D.P., and Vaucheret, H. (2005). Partially redundant functions of *Arabidopsis* DICER-like enzymes and a role for DCL4 in producing trans-acting siRNAs. Curr. Biol. *15*, 1494–1500.

Ho, S.N., Hunt, H.D., Horton, R.M., Pullen, J.K., and Pease, L.R. (1989). Site-directed mutagenesis by overlap extension using the polymerase chain reaction. Gene *77*, 51–59.

Howell, M.D., Fahlgren, N., Chapman, E.J., Cumbie, J.S., Sullivan, C.M., Givan, S.A., Kasschau, K.D., and Carrington, J.C. (2007). Genome-wide analysis of the RNA-DEPENDENT RNA POLYMERASE6/DICER-LIKE4 pathway in Arabidopsis reveals dependency on miRNA- and tasiRNA-directed targeting. Plant Cell *19*, 926–942.

Hunter, C., Sun, H., and Poethig, R.S. (2003). The *Arabidopsis* heterochronic gene *ZIPPY* is an ARGONAUTE family member. Curr. Biol. *13*, 1734–1739.

Hunter, C., Willmann, M.R., Wu, G., Yoshikawa, M., de la Luz Gutierrez-Nava, M., and Poethig, S.R. (2006). Trans-acting siRNA-mediated repression of ETTIN and ARF4 regulates heteroblasty in Arabidopsis. Development *133*, 2973–2981.

Jones-Rhoades, M.W., and Bartel, D.P. (2004). Computational identification of plant microRNAs and their targets, including a stress-induced miRNA. Mol. Cell *14*, 787–799.

Kasschau, K.D., Fahlgren, N., Chapman, E.J., Sullivan, C.M., Cumbie, J.S., Givan, S.A., and Carrington, J.C. (2007). Genome-wide profiling and analysis of Arabidopsis siRNAs. PLoS Biol. *5*, e57.

Kumagai, M.H., Donson, J., Della-Cioppa, G., Harvey, D., Hanley, K., and Grill, L.K. (1995). Cytoplasmic inhibition of carotenoid biosynthesis with virus-derived RNA. Proc. Natl. Acad. Sci. USA *92*, 1679–1683.

Li, C.F., Pontes, O., El-Shami, M., Henderson, I.R., Bernatavichute, Y.V., Chan, S.W., Lagrange, T., Pikaard, C.S., and Jacobsen, S.E. (2006). An ARGONAUTE4-containing nuclear processing center colocalized with Cajal bodies in Arabidopsis thaliana. Cell *126*, 93–106.

Liu, J., Valencia-Sanchez, M.A., Hannon, G.J., and Parker, R. (2005). MicroRNA-dependent localization of targeted mRNAs to mammalian P-bodies. Nat. Cell Biol. *7*, 719–723.

Llave, C., Xie, Z., Kasschau, K.D., and Carrington, J.C. (2002). Cleavage of Scarecrow-like mRNA targets directed by a class of *Arabidopsis* miRNA. Science *297*, 2053–2056.

Lu, C., Kulkarni, K., Souret, F.F., Muthuvalliappan, R., Tej, S.S., Poethig, R.S., Henderson, I.R., Jacobsen, S.E., Wang, W., Green, P.J., and Meyers, B.C. (2006). MicroRNAs and other small RNAs enriched in the Arabidopsis RNA-dependent RNA polymerase-2 mutant. Genome Res. *16*, 1276–1288.

Ma, J.B., Yuan, Y.R., Meister, G., Pei, Y., Tuschl, T., and Patel, D.J. (2005). Structural basis for 5′-end-specific recognition of guide RNA by the A. fulgidus Piwi protein. Nature *434*, 666–670.

Parker, J.S., Roe, S.M., and Barford, D. (2005). Structural insights into mRNA recognition from a PIWI domain-siRNA guide complex. Nature *434*, 663–666.

Peragine, A., Yoshikawa, M., Wu, G., Albrecht, H.L., and Poethig, R.S. (2004). SGS3 and SGS2/SDE1/RDR6 are required for juvenile development and the production of trans-acting siRNAs in *Arabidopsis*. Genes Dev. *18*, 2368–2379.

Qi, Y., Denli, A.M., and Hannon, G.J. (2005). Biochemical specialization within Arabidopsis RNA silencing pathways. Mol. Cell *19*, 421–428.

Qi, Y., He, X., Wang, X.J., Kohany, O., Jurka, J., and Hannon, G.J. (2006). Distinct catalytic and non-catalytic roles of ARGONAUTE4 in RNA-directed DNA methylation. Nature *443*, 1008–1012.

Rivas, F.V., Tolia, N.H., Song, J.J., Aragon, J.P., Liu, J., Hannon, G.J., and Joshua-Tor, L. (2005). Purified Argonaute2 and an siRNA form recombinant human RISC. Nat. Struct. Mol. Biol. *12*, 340–349.

Ronemus, M., Vaughn, M.W., and Martienssen, R.A. (2006). MicroRNA-targeted and small interfering RNA-mediated mRNA degradation is regulated by argonaute, dicer, and RNA-dependent RNA polymerase in Arabidopsis. Plant Cell *18*, 1559–1574.

Ruby, J.G., Jan, C., Player, C., Axtell, M.J., Lee, W., Nusbaum, C., Ge, H., and Bartel, D.P. (2006). Large-scale sequencing reveals 21U-RNAs and additional microRNAs and endogenous siRNAs in C. elegans. Cell *127*, 1193–1207.

Schwab, R., Palatnik, J.F., Riester, M., Schommer, C., Schmid, M., and Weigel, D. (2005). Specific effects of microRNAs on the plant transcriptome. Dev. Cell *8*, 517–527.

Steiner, F.A., Hoogstrate, S.W., Okihara, K.L., Thijssen, K.L., Ketting, R.F., Plasterk, R.H., and Sijen, T. (2007). Structural features of small RNA precursors determine Argonaute loading in Caenorhabditis elegans. Nat. Struct. Mol. Biol. *14*, 927–933.

Sunkar, R., and Zhu, J.K. (2004). Novel and stress-regulated microRNAs and other small RNAs from *Arabidopsis*. Plant Cell *16*, 2001–2019.

Talmor-Neiman, M., Stav, R., Klipcan, L., Buxdorf, K., Baulcombe, D.C., and Arazi, T. (2006). Identification of trans-acting siRNAs in moss and an RNA-dependent RNA polymerase required for their biogenesis. Plant J. *48*, 511–521.

Tolia, N.H., and Joshua-Tor, L. (2007). Slicer and the argonautes. Nat. Chem. Biol. *3*, 36–43.

Tomari, Y., Du, T., and Zamore, P.D. (2007). Sorting of Drosophila small silencing RNAs. Cell *130*, 299–308.

Vazquez, F., Vaucheret, H., Rajagopalan, R., Lepers, C., Gasciolli, V., Mallory, A.C., Hilbert, J.L., Bartel, D.P., and Crete, P. (2004). Endogenous trans-acting siRNAs regulate the accumulation of *Arabidopsis* mRNAs. Mol. Cell *16*, 69–79.

Xie, Z., Allen, E., Wilken, A., and Carrington, J.C. (2005). DICER-LIKE 4 functions in trans-acting small interfering RNA biogenesis and vegetative phase change in *Arabidopsis thaliana*. Proc. Natl. Acad. Sci. USA *102*, 12984–12989.

Yoshikawa, M., Peragine, A., Park, M.Y., and Poethig, R.S. (2005). A pathway for the biogenesis of trans-acting siRNAs in *Arabidopsis*. Genes Dev. *19*, 2164–2175.

Zhang, X., Yuan, Y.R., Pei, Y., Lin, S.S., Tuschl, T., Patel, D.J., and Chua, N.H. (2006). Cucumber mosaic virus-encoded 2b suppressor inhibits Arabidopsis Argonaute1 cleavage activity to counter plant defense. Genes Dev. *20*, 3255–3268.

Zilberman, D., Cao, X., and Jacobsen, S.E. (2003). ARGONAUTE4 control of locus-specific siRNA accumulation and DNA and histone methylation. Science *299*, 716–719.